?

Effects of Large-Scale Convection on p-mode Frequencies

M. Swisdak and E. Zweibel
JILA, University of Colorado, Boulder, CO 80309-0440

ABSTRACT

We describe an approach for finding the eigenfrequencies of solar acoustic modes (p modes) in a convective envelope in the WKB limit. This approximation restricts us to examining the effects of fluid motions which are large compared to the mode wavelength, but allows us to treat the three-dimensional mode as a localized ray. The method of adiabatic switching is then used to investigate the frequency shifts resulting from simple perturbations to a polytropic model of the convection zone as well as from two basic models of a convective cell. We find that although solely depth-dependent perturbations can give frequency shifts which are first order in the strength of the perturbation, models of convective cells generate downward frequency shifts which are second order in the perturbation strength. These results may have implications for resolving the differences between eigenfrequencies derived from solar models and those found from helioseismic observations.

1. Introduction

Comparisons between eigenfrequencies of solar acoustic modes (also known as p modes, since pressure provides the restoring force) determined from solar models and eigenfrequencies measured via helioseismology show that our understanding of the Sun's structure is incomplete (Gough *et al.* 1996). In particular, the model frequencies show the largest discrepancies in three distinct regions: near the solar core, at the tachocline (the boundary between the radiative interior and the convective envelope), and near the solar surface. In this work, we focus on the discrepancy near the solar surface, which is thought to be partially a consequence of the incomplete modeling of convective effects in solar models.

In standard solar models, the stratification of the convection zone is determined by mixing-length theories in which one lengthscale is used to parameterize all convective motions. In reality, the outer portions of the convection zone harbor turbulent convection on scales at least as small as granules (1 Mm) and as big as supergranules (20–30 Mm). In addition, cells spanning the entire convection zone (200 Mm) may also exist. These turbulent motions affect the frequencies and linewidths of p modes, but in a manner which is not yet fully understood. Most authors (for example, Brown 1984, Lavely & Ritzwoller 1993, Gruzinov 1998) treat the

lengthscales of convective motions as small compared to the mode wavelengths. By parameterizing the effects of convection as a turbulent pressure, they are able to average over the motions of individual cells, thereby simplifying the analysis. Our work lies at the opposite limit. We assume that the wavelengths of the modes are small compared to the lengthscale of the convection. This formulation allows us to work in the WKB limit and treat the modes as rays following trajectories identical to those of classical particles.

Working in the WKB limit also allows us to use the formalism of Hamiltonian mechanics to find the p-mode eigenfrequencies given a model of the convective envelope. We introduce two related methods of doing so, EBK (Einstein–Brillouin–Keller) quantization and adiabatic switching. After showing that adiabatic switching is better suited for finding the eigenfrequencies of complex systems, we apply it to a few simple examples of convective envelopes.

We find that for convective envelopes the fractional frequency shift scales as the square of the ratio of the convective velocity v to the sound speed c. The frequency shift averages to zero to first order in v/c and is downshifted to second order because the ray spends more time in the region of negative Doppler shift (Brown 1984). A downshift is produced by temperature fluctuations for similar reasons. Roughly,

$$-\delta\omega/\omega \sim v^2/c^2 \tag{1}$$

where $\delta\omega$ is the change in the eigenfrequency ω. Evaluating c at the midpoint of a p mode cavity gives

$$-\delta\omega/\omega \sim \frac{v^2}{gR_\odot}\ell \sim (v_1/400)^2\ell \tag{2}$$

where v_1 is the convective velocity in km/s and ℓ is the mode degree. For typical velocities of 0.3 km/s at a depth of 10 Mm (the cavity midpoint of a $n = 1$, $\ell = 200$ p mode), the fractional frequency shift is $\approx 10^{-4}$. Larger ℓ values will produce larger shifts. Observational determinations of p-mode eigenfrequencies quote error bars of $\delta\omega/\omega \approx 5 \times 10^{-4}$, suggesting that this mechanism could produce a detectable shift.

We develop the problem, present the theoretical justification for the ray approximation, and provide necessary concepts from Hamiltonian theory in §2. In §3 we describe two methods for finding the eigenfrequencies of convective envelopes, EBK quantization and adiabatic switching. Our results for three convective structures, a vertical sound speed perturbation and two simple models of convective cells, are presented in §4. In §5 we discuss our results and outline several possible extensions of the work.

2. Theoretical Background

Like an organ pipe, the Sun has resonant modes of oscillation (see Gough & Toomre 1991 for a review). Each eigenmode is denoted, in a manner similar to the designation of orbitals in the hydrogen atom, by its radial order n, spherical harmonic degree ℓ, and azimuthal order m.

Although in general the eigenfrequency ω associated with each mode depends on n, ℓ, and m, the assumption of spherical symmetry in a model creates a degeneracy so that ω is independent of m. In the Sun, rotation breaks the spherical symmetry and hence the degeneracy.

Solar acoustic modes are radially confined within a resonant cavity by the sound speed structure and stratification of the solar interior (the exception being modes with $\ell = 0$ which penetrate to $r = 0$). As ℓ increases at fixed n, the inner turning point of a mode moves outward in radius. Although there is some dependence on n, the resonant cavities of p modes with $\ell \gtrsim 60$ lie completely within the convection zone and we expect that these modes are most strongly affected by convective structures. Since we are primarily interested in the turbulent convection near the solar surface, we will consider oscillations with $\ell \gtrsim 200$ which are trapped within the outer 10% (by radius) of the Sun.

Instead of treating the complete problem of the effects of convective structures of arbitrary scale on the structure and frequencies of high-ℓ modes, we limit the problem still further. Following the lead of time-distance helioseismology (Duvall *et al.* 1993), we approximate the three-dimensional mode as a localized ray, in the process losing any information concerning perturbations in the structure of the mode, but allowing the ray to be described as a Hamiltonian system. In order to make this simplification — equivalent to the limits of geometrical acoustics (Landau & Lifshitz 1959) and the WKB approximation — we must restrict ourselves to considering the effects of convective structures which are large compared to the wavelength of the mode.

2.1. The Modal Equation

We begin with the linearized equations of hydrodynamics for the vector displacement $\delta\mathbf{r}$ of a fluid parcel. The continuity equation is

$$\rho' + \nabla \cdot (\rho\, \delta\mathbf{r}) = \delta\rho + \rho \nabla \cdot (\delta\mathbf{r}) = 0 \tag{3}$$

and the momentum equation is

$$\rho \frac{\partial^2 \delta\mathbf{r}}{\partial t^2} = -\nabla p' + \rho \mathbf{g}' + \rho' \mathbf{g}, \tag{4}$$

where δf and f' are the Lagrangian and Eulerian perturbations to an equilibrium quantity f, and are related through $\delta f = f' + (\delta\mathbf{r} \cdot \nabla) f$. The density, pressure, and gravity are denoted by ρ, p, and $\mathbf{g}$ respectively where boldface symbols denote vector quantities. Throughout this work all fluid motions are assumed to be adiabatic, hence the density and pressure perturbations are connected by

$$\delta p = \frac{\Gamma_1\, p}{\rho} \delta\rho, \tag{5}$$

where the adiabatic exponent

$$\Gamma_1 \equiv \left(\frac{\partial \ln p}{\partial \ln \rho} \right)_s \tag{6}$$

with the subscript s indicating that the derivative is taken at constant specific entropy. Finally, Poisson's equation relates $\mathbf{g}'$ and ρ':

$$\nabla \cdot \mathbf{g}' = -4\pi G\rho', \tag{7}$$

where G is the Newtonian gravitational constant.

Furthermore, in order to simplify the calculations we:

1. Assume a plane-parallel geometry. We are concerned with high-degree modes which are trapped close to the surface and feel the curvature of the Sun only as a small perturbation. This assumption allows us to treat the equilibrium gravitational acceleration as a constant: $\mathbf{g} = g\hat{\mathbf{z}}$.

2. Assume the region of propagation takes the form of a two-dimensional slab. The vertical coordinate, increasing inwards from the surface, is given by z and the horizontal coordinate is x. The horizontal length of the slab, L, is the Sun's circumference: $L = 2\pi R_\odot$. Finally, we assume periodic boundary conditions in the horizontal direction so that $f|_{x=0} = f|_{x=L}$ for any variable f.

3. Neglect perturbations to the gravitational acceleration so that $\mathbf{g}' = 0$. This is known as the Cowling approximation and is justified when either n or ℓ are large (Cowling 1941), the latter being the case in this work.

It has been shown (Gough 1993) that, given the above assumptions, the system of equations (3)–(7) can be reduced to a single equation for the variable $\Psi = -\rho^{-1/2}\delta p = c^2\rho^{1/2}\nabla \cdot \delta\mathbf{r}$:

$$\left(\frac{\partial^2}{\partial t^2} + \omega_c^2\right)\frac{\partial^2\Psi}{\partial t^2} - c^2\frac{\partial^2}{\partial t^2}\nabla^2\Psi - c^2N^2\nabla_h^2\Psi = 0, \tag{8}$$

where ∇_h^2 is the horizontal Laplacian operator and

$$c^2 \equiv \frac{\Gamma_1 p}{\rho} \tag{9}$$

is the adiabatic sound speed. The acoustic cutoff frequency ω_c is defined by

$$\omega_c^2 \equiv \frac{c^2}{4H^2}(1 + 2\hat{\mathbf{z}} \cdot \nabla H_\rho) \tag{10}$$

where

$$H_\rho \equiv \left(\frac{d\ln\rho}{dz}\right)^{-1} \tag{11}$$

is the density scale height. The buoyancy, or Brunt-Väisälä, frequency N is defined by

$$N^2 \equiv g\left(\frac{1}{H_\rho} - \frac{g}{c^2}\right) \tag{12}$$

with $N^2 < 0$ corresponding to convective instability.

A complete solution of equation (8) yields both p and g modes, the latter having buoyancy as their restoring force. Since the solar convection zone is nearly adiabatically stratified, we have $N^2 \approx 0$ there. Neglecting the third term in equation (8) so that only p modes are allowed, we arrive at a modified wave equation

$$\left(\frac{\partial^2}{\partial t^2} + \omega_c^2\right)\Psi - c^2\nabla^2\Psi = 0. \tag{13}$$

Note that both c and ω_c can be functions of position.

2.2. The Ray Approximation

At this point, equation (13) may still be solved as an eigenvalue problem for the structure and eigenfrequencies of the p modes. In order to consider the problem in the ray limit, we must make one further approximation. Consider, for the moment, a simple solar model where $\omega_c = 0$ and c is a constant. Equation (13) then reduces to the Helmholtz equation, which has a plane-wave solution

$$\Psi = \Psi_0 e^{i(\mathbf{k}\cdot\mathbf{r} - \omega t)}. \tag{14}$$

The ray associated with this plane wave follows a trajectory perpendicular to the wavefronts.

Now, consider instead a system where the wavelength of the mode is much shorter than the lengthscale over which equilibrium quantities (such as c, p and ρ) vary. Letting the ratio of these lengthscales be denoted by Λ^{-1} — which we treat as a constant, small parameter — we write the solution to equation (13) as a plane wave with varying amplitude, Ψ_0, and phase, Φ:

$$\Psi = \Psi_0(\mathbf{r}, t)e^{i\Lambda\Phi(\mathbf{r},t)}. \tag{15}$$

Although we have not made any approximations thus far, the form of equation (15) suggests that Ψ is rapidly oscillating compared to the background state, implying a solution which may be thought of as locally planar. These planar wavefronts allow the motion to be approximated by a ray.

Using this *ansatz* and following the work of Gough (1993), we expand equation (13) and equate powers of Λ. This process is equivalent to the WKB approximation and gives the leading equation

$$\left(\frac{\partial\Phi}{\partial t}\right)^2 - \left(\frac{\omega_c}{\Lambda}\right)^2 - c^2\left|\frac{\partial\Phi}{\partial\mathbf{x}}\right|^2 = 0. \tag{16}$$

Next, making the analogy between equations (14) and (15), we define the local frequency ω and wavenumber $\mathbf{k}$ as

$$\omega \equiv -\Lambda\frac{\partial\Phi}{\partial t} \qquad \text{and} \qquad \mathbf{k} \equiv \Lambda\frac{\partial\Phi}{\partial\mathbf{x}} \tag{17}$$

These identifications allow us to write equation (16) in the form of a dispersion relation:

$$\omega = (c^2 k^2 + \omega_c^2)^{\frac{1}{2}}. \tag{18}$$

Furthermore, equation (17) also implies equations of motion:

$$\frac{d\mathbf{k}}{dt} = -\frac{\partial \omega}{\partial \mathbf{x}} \qquad \text{and} \qquad \frac{d\mathbf{x}}{dt} = \frac{\partial \omega}{\partial \mathbf{k}}, \tag{19}$$

where $\frac{d}{dt}$ denotes the derivative with respect to time along a ray path.

Equations (19) are Hamilton's equations for a Hamiltonian $H = \omega$ in terms of the canonical positions $q_i = x_i$ and momenta $p_i = k_i$. The ray's dispersion relation, $\omega(\mathbf{x}, \mathbf{k}, t)$, is identified as the functional form of the Hamiltonian. While this result may appear serendipitous, it is well-known in quantum mechanics (Goldstein 1965) that high-frequency solutions to the wave equation (in other words, solutions which oscillate rapidly compared to any background variation) follow dynamics similar to classical particles.

2.3. Action variables and adiabatic invariants

The identification with Hamiltonian mechanics described in the preceding subsection allows us to take advantage of the extensive results available in the field. In this subsection, we review several results from Hamiltonian theory which will be used later. More details can be found in a number of classical mechanics texts (for example, Goldstein 1965, Arnol'd 1978, Lichtenberg & Lieberman 1983, Tabor 1989).

First, we present two results which follow from the structure of the governing equations. In any Hamiltonian system it is known that

$$\frac{dH}{dt} = \frac{\partial H}{\partial t}. \tag{20}$$

Hence, for systems where the Hamiltonian is not explicitly time-dependent, it is a constant of the motion. Second, if the Hamiltonian is cyclic (independent) of one of the canonical positions q_i, then the corresponding canonical momentum p_i is a constant of the motion:

$$\frac{\partial H}{\partial q_i} = 0 \qquad \text{implies} \qquad \frac{dp_i}{dt} = 0. \tag{21}$$

Certain special Hamiltonians, named integrable systems, have equal numbers of independent constants of the motion as degrees of freedom. Such systems allow a change of variables where all of the new canonical positions, termed angle variables, are cyclic. The new canonical momenta are the actions, I_k, and are defined as

$$I_k = \frac{1}{2\pi} \oint_{C_k} \mathbf{p} \cdot d\mathbf{q}, \tag{22}$$

for $k = 1, \ldots, n$, where n is the number of degrees of freedom of the system. The curves C_k are topologically-independent closed paths in phase space which do not have to be ray trajectories. Since the angles are cyclic, each action is a constant of the motion resulting in n total constants. Since a Hamiltonian system with n degrees of freedom has a $2n$-dimensional phase space, integrability ensures that the phase-space trajectories are confined to $(2n - n) = n$-dimensional surfaces which have the topology of n-dimensional tori. An integrable system is placed on a particular invariant torus by its initial conditions and cannot stray from this torus as the system evolves in time.

A concrete example is provided by the Hamiltonian of equation (18) in a two-dimensional geometry. The system has two degrees of freedom, so its phase space has four dimensions. If we assume that the Hamiltonian is independent of time, then the frequency ω is a constant. Furthermore, if we consider a system where c and ω_c are independent of one of the position coordinates, say x, then the corresponding wavenumber k_x is also a constant of the motion. The existence of these two constants ensures the integrability of the system and restricts phase-space motions to a two-dimensional surface, topologically equivalent to a two-dimensional torus.

General Hamiltonian systems, however, are usually non-integrable. The fate of invariant tori in non-integrable systems was addressed by the KAM (Kolmogorov-Arnol'd-Moser) theorem. It concerns systems which are nearly-integrable in the sense that they may be written as

$$H = H_0(\mathbf{I}) + \epsilon H_1(\mathbf{I}, \mathbf{\Theta}), \tag{23}$$

where $\mathbf{I}$ and $\mathbf{\Theta}$ are vectors of the action and angle coordinates, respectively, and ϵ is a small parameter. Roughly, the KAM theorem states that for sufficiently small values of ϵ, most invariant tori are preserved. In other words, for small perturbations from integrability, most sets of initial conditions remain on invariant tori. However, the destroyed tori are distributed throughout the invariant ones in phase space and as the perturbation increases, their density increases. For a strong enough perturbation, no invariant tori remain.

3. Methods

Having shown that within the WKB approximation we may treat p modes as a Hamiltonian system, the powerful techniques developed for such systems become available for our use. Instead of solving the eigenvalue problem of equation (13), we seek the eigenfrequencies of the Hamiltonian given by equation (18). However, equations (19) describe the motion of any ray; we do not know *a priori* which rays correspond to eigenmodes. We consider two methods of isolating the systems corresponding to eigenmodes: EBK quantization and the method of adiabatic switching. Both of these methods have been used in chemical physics to understand molecular spectra (Patterson 1985, Shirts *et al.* 1987). Gough (1993) discussed EBK quantization of stellar waves but did not fully implement the method.

In this paper we are interested in finding the eigenfrequencies of non-integrable systems which can be expressed as a perturbation to an integrable system as in equation (23). Our base solar state, corresponding to H_0 in equation (23) and which we will show below to be integrable, will be a two-dimensional, adiabatically stratified, plane-parallel polytrope. Polytropic systems are those where the pressure p and density ρ are assumed to be related by

$$\frac{p}{p_0} = \left(\frac{\rho}{\rho_o}\right)^{1+\frac{1}{\mu}}, \tag{24}$$

where p_0 and ρ_0 are constants and μ is the polytropic index, which for an adiabatically stratified system may be written as $\mu = 1 + 1/\Gamma_1$ in terms of the adiabatic exponent defined in equation (6). The outer portion of the solar convection zone is well-approximated by a polytrope with $\mu \approx 3$.

Enforcing hydrostatic equilibrium leads to the relations

$$\frac{p}{p_0} = \left(\frac{z}{z_0}\right)^{\mu+1} \qquad \text{and} \qquad \frac{\rho}{\rho_0} = \left(\frac{z}{z_0}\right)^{\mu} \tag{25}$$

where z_0 is a constant. Finally, the adiabatic sound speed and cutoff frequency are given by

$$c^2 = \frac{gz}{\mu} \qquad \text{and} \qquad \omega_c^2 = \frac{\mu(\mu+2)}{4z^2}c^2 \tag{26}$$

where g is the gravitational acceleration.

Figure 1 shows a sample raypath in an adiabatically stratified, two-dimensional polytropic envelope with periodic horizontal boundary conditions and $\mu = 3$. The vertical structure of this ray corresponds to a mode with $n = 1$, $\ell = 200$ (see below for a description of the mode numbers); however, the horizontal structure has been altered for legibility – it is equivalent to a mode with $n = 1, \ell = 12$. If drawn to scale, the box would be a thin ribbon, with an aspect ratio of $\approx 300 : 1$. Furthermore, the ray would fit ≈ 80 horizontal wavelengths into the box instead of ≈ 5 as displayed. The ray is confined in the vertical direction by two boundaries, or caustic surfaces, where $k_z = 0$. If we continue to trace the ray, it will eventually fill the entire cavity.

3.1. EBK quantization

While finding the eigenvalues of a Hamiltonian is usually considered as a quantum-mechanical problem, historically it was first approached from the standpoint of classical mechanics. The quantization which led to the Bohr model of the hydrogen atom was an early attempt to find eigenvalues through the quantization of the action (in this case, the orbital angular momentum). Later refinements resulted in EBK semi-classical quantization (Einstein 1917, Brillouin 1926, Keller 1958) which states that the action I_k of equation (22) is quantized:

$$I_k = \frac{1}{2\pi}\oint_{C_k} \mathbf{p}\cdot d\mathbf{q} = \left(n_k + \frac{m_k}{4}\right). \tag{27}$$

The quantum numbers n_k and m_k are non-negative integers, with m_k representing the number of caustic surfaces (those surfaces which define the envelope of possible trajectories) crossed by C_k.

As an example of EBK quantization, consider the polytropic envelope described above. Christensen-Dalsgaard (1980) showed that the eigenfrequencies for this system are given by

$$\omega^2 = \frac{2gk_x}{\mu}\left(n + \frac{\mu}{2}\right) \qquad \text{for} \qquad n = 1, 2, ... \tag{28}$$

where $k_x = \ell/R_\odot$ where $R_\odot$ is the solar radius and ℓ is an integer. The latter condition arises from requiring that ℓ wavelengths fit around the Sun's circumference.

EBK quantization can nearly reproduce these results. Combining the expressions for c^2 and ω_c^2 from equation (26) with the dispersion relation of equation (18), we may solve for k_z:

$$k_z^2 = \frac{\omega^2 - \omega_c^2}{c^2} - k_x^2 = \frac{\mu\omega^2}{gz} - \frac{\mu^2}{4z^2}\left(1 + \frac{2}{\mu}\right) - k_x^2, \tag{29}$$

However, ω is constant since the dispersion relation does not explicitly depend on time. Furthermore, k_x is also constant since the unperturbed quantities are independent of x. Evaluating equation (27) on a curve of constant x, and noticing that this curve touches two caustics, one each at the top and bottom of the cavity, we have

$$I_z = \frac{1}{\pi}\int_{z_1}^{z_2} k_z dz = \left(n - \frac{1}{2}\right) \qquad \text{for} \qquad n = 1, 2, \ldots \tag{30}$$

where z_1 and z_2 are the upper and lower turning points of the ray. With k_z given by equation (29), the integral in equation (30) can be done analytically. The final result is

$$\omega^2 = \frac{2gk_x}{\mu}\left[n - \frac{1}{2} + \frac{\mu}{2}\left(1 + \frac{2}{\mu}\right)^{\frac{1}{2}}\right] \qquad \text{for} \qquad n = 1, 2, \ldots \tag{31}$$

If we also evaluate equation (27) on a curve of constant z, we see that the curve touches no caustics and hence

$$I_x = \frac{1}{2\pi}\int_0^{2\pi R_\odot} k_x dx = \ell \qquad \text{for} \qquad \ell = 0, 1, \ldots \tag{32}$$

This gives:

$$k_x = \frac{\ell}{R_\odot} \qquad \text{for} \qquad \ell = 0, 1, \ldots \tag{33}$$

Equation (33) is the correct horizontal quantization condition. Equations (28) and (31) for the vertical quantization are not the same, however. Taking $n = 1$ and $\mu = 3/2$, the relative error in the eigenfrequencies is $\approx 6\%$, with the agreement improving as either n or μ increase. The magnitude of this error is much larger than the accuracy to which the true p-mode eigenfrequencies may be determined. However, we are investigating frequency *shifts*, not magnitudes, and so the

small differences between EBK frequencies and the true frequencies are expected to have only a small effect on our results.

While EBK quantization appears to be a fruitful method for determining the eigenfrequencies, it is not generally applicable. Analytically evaluating the quantization conditions of equations (30) and (32) for all but extremely simple expressions for the sound speed and cutoff frequency is difficult. In particular, if these parameters depend on x, the horizontal wavenumber k_x is not a constant of the motion and the evaluation of the integrals is impractical.

An alternate approach implements the quantization conditions by propagating the ray trajectories and evaluating equations (30) and (32) numerically. By thoughtfully choosing the paths C_k, the EBK equations may be reduced to quantizing the areas of Poincaré surface of sections (phase space slices in the p_i-q_i plane). While Noid and Marcus (1975) used this approach with some success to find the energy levels of an anharmonically coupled pair of oscillators, it is not optimal for many non-integrable systems. As such systems move farther from integrability, increasing numbers of invariant tori are destroyed. The initial conditions corresponding to these tori are then free to wander in phase space, giving the surfaces of section a characteristic "fuzzy" appearance, an early example of which is seen in the work of Hénon and Heiles (1964). The form of these surfaces of section makes numerical determination of their areas very difficult. Consequently, we seek another method for implementing the EBK quantization rules for non-integrable systems.

3.2. Adiabatic Switching

Ehrenfest (1917) was among the first to propose the concept of adiabatic switching, although his work has been superseded by modern treatments. In essence, his hypothesis was that if a system is changed in a reversible, adiabatic way, then allowed motions will be smoothly transformed to allowed motions. In the language of §2.3, this is analogous to saying that a system will remain on an invariant torus if it is altered in a smooth manner. A thorough review of the modern implementation of the method of adiabatic switching and its applications can be found in Skodje & Cary (1988).

In adiabatic switching, the system is initialized in an eigenstate of a integrable Hamiltonian for which the eigenfrequencies are known. The system is allowed to evolve as the strength of a perturbation (not necessarily small, although small in our case) to the original Hamiltonian is slowly increased, eventually leaving the system under the direction of a new, usually non-integrable, Hamiltonian for which the eigenfrequencies are not known. Due to the adiabatic nature of the switch, however, the original eigenstate has slowly relaxed into an eigenstate of the new system from which the new eigenfrequency can then be determined.

While adiabatic switching has been used extensively, for example, to determine the energy levels of systems with many degrees of freedom in complicated external electromagnetic fields, it does not have a complete mathematical justification. For systems with one degree of freedom, it is

known that the action is an adiabatic invariant which remains constant under slow perturbations to the Hamiltonian, where "slow" means "long with respect to other characteristic timescales of the problem". In the language of §2.3, the initial invariant torus can be deformed into an invariant torus of the final state. For systems with more than one degree of freedom, no such theorem exists and the overall dynamics are not as well understood. In particular, the KAM theorem tells us that some invariant tori of the initial system will be destroyed with the introduction of non-integrability. What happens when the system switches through such destroyed tori, found everywhere in phase space, is not known in general.

Despite these considerations, the empirical justification for adiabatic switching is quite strong. Skodje & Cary (1988) explore these and other difficulties and conclude that, with some precautions, adiabatic switching is an excellent method for implementing EBK quantization in non-integrable systems.

The mathematical formulation of adiabatic switching is fairly straightforward. The non-integrable Hamiltonian for which the eigenfrequencies are desired, which in our case is a function of position and wavenumber, is written as a sum of two terms

$$H(\mathbf{x}, \mathbf{k}) = H_0 + H_1, \tag{34}$$

where H_0 is an integrable Hamiltonian for which the eigenfrequencies are known from EBK quantization and H_1 is a term which includes everything else. Into equation (34), we introduce a time-dependent switching function $\lambda(t)$:

$$H(\mathbf{x}, \mathbf{k}) = H_0 + \lambda(t) H_1 \tag{35}$$

which satisfies

$$\lambda(0) = 0 \qquad \text{and} \qquad \lambda(T) = 1 \tag{36}$$

for some time T which, in order to ensure that the transition from H_0 to H is adiabatic, is taken to be much longer than other timescales associated with the system (for instance, the characteristic propagation time $t_{ray} \approx \omega^{-1}$). In addition, λ is chosen such that its first few derivatives are continuous at the endpoints. In this work, λ is taken to be

$$\lambda(t) = \frac{t}{T} - \frac{1}{2\pi} \sin\left(\frac{2\pi t}{T}\right). \tag{37}$$

Johnson (1985) has a discussion of the effects of different switching functions.

At $t = 0$ our initial conditions are such that we satisfy the EBK quantization conditions for the Hamiltonian H_0. We then numerically integrate Hamilton's equations of motion (19) under the influence of the Hamiltonian H given in equation (35). As t increases so does $\lambda(t)$, adiabatically switching on the non-integrable term H_1, and allowing the eigenfrequency of the system to slowly adjust from its original value. At $t = T$ we arrive at the eigenfrequency of the full Hamiltonian H.

3.3. Numerical Methods

For our reference state H_0, we use the plane-parallel, adiabatically stratified polytrope whose EBK eigenfrequencies are given by equation (31). In order to expand our investigation to convective motions, we include a Doppler term in the Hamiltonian of equation (18):

$$\omega - \mathbf{k} \cdot \mathbf{v} = (c^2 k^2 + \omega_c^2)^{\frac{1}{2}} \tag{38}$$

where $\mathbf{v}$ is the velocity field which is taken to be zero for the reference state.

Writing the Hamiltonian in the form of equation (35), we have:

$$\omega = c_0 \left(k^2 + \frac{\mu(\mu+2)}{4z^2} \right)^{\frac{1}{2}} + \lambda(t) \left[(c - c_0) \left(k^2 + \frac{\mu(\mu+2)}{4z^2} \right)^{\frac{1}{2}} + \mathbf{k} \cdot \mathbf{v} \right] \tag{39}$$

where c_0 is the polytropic sound speed and the cutoff frequency of equation (26) has been used for ω_c. The true definition of the cutoff frequency, given in equation (10), also involves the density scale height H_ρ which, in a consistent model, will be perturbed when the sound speed is perturbed. However, this effect should be small and we assume in this work that H_ρ keeps its polytropic value of z/μ, independent of any perturbations to c.

Although we have analytic expressions for the sound speed and velocities of the final states in the examples we consider below, we anticipate that in future applications we will not. In preparation, we discretize the propagation region and specify the sound speed and velocity fields at each point. The size of the discretization element was determined through numerical experimentation.

In order to integrate equations (19), the code uses a slightly-modified version of the DE package of Shampine & Gordon (1975): a variable-order, variable-timestep Adams-Moulton-Bashforth PECE method. This method allows the user to specify tolerances for both the absolute and relative error. We found that the integration was sufficiently accurate and quick if both were set to 10^{-5}.

We have not yet addressed how to choose the switching time T of equation (37). In order to ensure adiabaticity, we must choose T to be much longer than the longest dynamical timescale associated with the system, in our case the time to complete one horizontal period. At first glance it may appear that, with infinite computer resources, increasingly better results may be gained by letting $T \to \infty$. This is not the case, however. Recall that the KAM theorem guarantees that some tori will be destroyed with any perturbation away from integrability (although most tori remain invariant for small perturbations). If the system switches through one of the destroyed tori and remains there for an extended period, the trajectory will begin to wander through phase space in a process called Arnold diffusion (Lichtenberg & Lieberman 1983). The rate of Arnold diffusion depends on the strength of the perturbation, but it is always present. Thus, the choice of T is also bounded from above. Following the lead of other investigators, we choose T to be ≈ 40 horizontal periods.

Beginning from different initial conditions on the same invariant torus should, in principle, lead to identical eigenfrequencies for the final state. Our numerical experiments found a small scatter, presumably arising from the Arnold diffusion described above. This scatter is observed by other investigators and it has been found empirically, although there is some mathematical justification presented in Skodje & Cary (1988), that better results are obtained by implementing the procedure for several randomly distributed initial conditions and averaging the final eigenvalues. We typically average 20 such initial states in this work, a number which we find suitably constrains the result. A typical integration of one trajectory takes ≈ 1 hour to complete on a 194 MHz SGI Power Onyx.

Finally, we have scaled our variables in order to simplify the numerics. All lengths are quoted in units of 10^9 cm and all times in units of $10^{2.5}$ seconds. For example, the solar surface gravity is $g = 2.7397$ and the Sun's radius is $R_\odot = 69.599$.

4. Results

Having outlined the method of adiabatic switching, we now apply it to several examples. Although we only consider fairly elementary problems in this work, adiabatic switching can in principle be applied to arbitrarily complex sound speed and velocity distributions. However, we believe that even the application to the simple systems considered here is new. The major physical constraint arises from the ray approximation made in §2.2 which allowed us to write the system in Hamiltonian form. Because of this approximation the validity of the method is restricted to systems where the perturbations from the reference state are large compared to the lengthscale of the mode, k^{-1}.

4.1. Height-Dependent Sound Speed Perturbation

We first explore an envelope with only a vertical perturbation to the sound speed and no velocity perturbation. The horizontal invariance of the final state implies that k_x is a constant of the motion and hence that the system is integrable at point during the switching. Since all intermediate invariant tori exist, we expect adiabatic switching to work quite well. For a reasonably-chosen perturbation we can check our results using EBK quantization. In order to compare the two methods, we:

1. Choose the initial conditions so that the system is in one of the quantized states given by equation (31).
2. Use the method of adiabatic switching to calculate the eigenfrequency of the new system using the perturbation described below.
3. Use equation (27) to calculate numerically the eigenfrequency of the new, perturbed system and compare with the results from adiabatic switching.

Consider the simple, but not particularly realistic, case where the sound speed is close to the polytropic version given by equation (26):

$$c = \left(\frac{gz}{\mu}\right)^{\frac{1}{2}} \left[1 + \epsilon \sin(\kappa z)\right], \tag{40}$$

where ϵ is a small parameter characterizing the sound speed variation and κ is the perturbation wavenumber. For the ray approximation to be valid we must have $\kappa \ll k_z$, a requirement which can only be met over part of the trajectory since $k_z = 0$ at the upper and lower turning points of the cavity. This difficulty is merely the well-known breakdown of the WKB approximation near the classical turning points. We will only require that $\kappa \ll k_z$ over most of the vertical extent of the cavity.

The acoustic cutoff frequency of equation (26) will also change to

$$\omega_c = \left(\frac{g(\mu+2)}{4z}\right)^{\frac{1}{2}} \left[1 + \epsilon \sin(\kappa z)\right], \tag{41}$$

As mentioned in §3.3, we ignore any accompanying perturbation to the density scale height H_ρ arising from the sound speed perturbation.

We compute relative frequency shifts, $\delta\omega/\omega$, via adiabatic switching and EBK quantization and list the results in Table 1. Even for $\epsilon = 0.16$, there is no appreciable difference in the frequency shifts. When applying adiabatic switching to non-integrable systems, however, we expect the trajectory to diffuse in phase space as invariant tori disappear, and thus the computed frequency shifts will be less accurate as we increase the perturbation strength.

A closer inspection of Table 1 reveals two interesting trends. First, all frequency shifts are positive, and second, as the final five rows demonstrate, the frequency shift is essentially linear in the perturbation parameter ϵ. Following the analysis of Gough (1993), we can explore both of these effects by expanding the EBK quantization condition of equation (30). We write the shifted frequency as $\omega = \omega_0 + \delta\omega$, where ω_0 is the unperturbed frequency. Similarly, we have from equation (40)

$$c = c_0 + \delta c = \left(\frac{gz}{\mu}\right)^{\frac{1}{2}} + \epsilon \left(\frac{gz}{\mu}\right)^{\frac{1}{2}} \sin(\kappa z) \tag{42}$$

where c_0 is the polytropic sound speed.

Applying the EBK quantization of equation (30) to the final state yields

$$\int_{z_1}^{z_2} k_z dz = \int_{z_1}^{z_2} \left[\frac{(\omega_0 + \delta\omega)^2 - \omega_c^2}{(c_0 + \delta c)^2} - k_x^2\right]^{\frac{1}{2}} dz = \frac{\pi}{2}, \tag{43}$$

where we have selected the mode with $n = 1$, ignored any perturbations to the cutoff frequency, and taken the integral over the original cavity (which is assumed to remain unperturbed). Next,

assuming that $\delta\omega$ and δc are small parameters, we expand and discard higher-order terms. After rearranging, we have

$$\int_{z_1}^{z_2} k_{z,0}\left[1+\frac{2}{c_0^2k_{z,0}^2}\left(\omega_0\delta\omega-\omega_0^2\frac{\delta c}{c_0}+\omega_c^2\frac{\delta c}{c_0}\right)\right]^{\frac{1}{2}}dz=\frac{\pi}{2}, \tag{44}$$

where $k_{z,0}$ is the positive root of equation (29). We expand again and cancel the zeroth-order term, leaving (after some algebraic simplifications)

$$\frac{\delta\omega}{\omega_0}=\left[\int_{z_1}^{z_2}\frac{\delta c}{c_0}\frac{k_0^2}{k_{z,0}}dz\right]\left[\int_{z_1}^{z_2}\frac{\omega_0^2}{c_0^2k_{z,0}}dz\right]^{-1}. \tag{45}$$

Thus, in a rough sense, $\delta\omega$ is related to the integral of δc over the cavity. In particular, since δc as given in equation (42) depends linearly on ϵ, we expect the same to be true of $\delta\omega$, an expectation confirmed by adiabatic switching. Furthermore, since every other term in equation (45) is non-negative, the sign of the frequency shift is determined by the sign of the integral of δc over the cavity.

Figure 2 shows the sound speed perturbation for the parameters $\epsilon = 0.01$ and $\kappa = 0.10$. The dashed lines indicate the vertical extent of the unperturbed resonant cavity. The perturbation is positive through the cavity, leading to the upward frequency shifts displayed in Table 1.

4.2. Cell-like Velocity Perturbation

In both this subsection and the next we will explore simple models of a convective cell. While the structure of the cell in §4.3 is more realistic, its complexity hides some important physical results. So, as a first attempt we model a convective cell as a velocity perturbation with no accompanying sound speed perturbation. Our velocity field is derived from a stream function

$$\mathbf{v}=\hat{\mathbf{y}}\times\nabla\left[\epsilon\sin\left(\frac{2\pi x}{L}\right)\sin\left(\frac{2\pi(z+b)}{L}\right)\right] \tag{46}$$

where $L = 2\pi R_\odot$ is the length of the cavity, ϵ and b are constants, and $\hat{\mathbf{y}}$ is a unit vector perpendicular to the previously-defined x- and z-axes.. Although this parameterization, by assuming incompressibility, violates the conservation of mass flux, we are more concerned with the physical insight we can derive from this model than its self-consistency. Expanding equation (46) gives the velocity field

$$v_x=\frac{\epsilon}{R_\odot}\sin\left(\frac{x}{R_\odot}\right)\cos\left(\frac{z+b}{R_\odot}\right)\qquad\text{and}\qquad v_z=-\frac{\epsilon}{R_\odot}\cos\left(\frac{x}{R_\odot}\right)\sin\left(\frac{z+b}{R_\odot}\right). \tag{47}$$

Figure 3 shows the streamlines for the velocity profile given by equation (47) with $b = 3$. The two dashed lines near the top of the plot delineate the resonant cavity of the initial eigenstate.

The WKB criterion is clearly met in the vertical direction. The streamlines close at lower depths, which are not shown in order to better resolve the cavity. Units for the x- and z-axes are those given in §4.1 and the contours in each plot are linearly spaced.

For all values of b except integer multiples of $2\pi R_\odot$, the vertical velocity is unphysically non-zero at $z = 0$. However, we can see from Figure 3 that by varying b, the effects of propagation through different portions of the convective cell are easily studied. We make the offset parameter b non-dimensional by defining

$$\phi = \frac{b + z_c}{R_\odot} \tag{48}$$

where z_c is the mean depth of the resonant cavity. The method of adiabatic switching is then used to investigate the dependence of eigenfrequencies on the parameters ϵ and b. Our results are shown in Table 2.

Clearly the frequency shift depends on the strength of the perturbation in a different manner than the system we considered in the previous section. Instead of a linear dependence, the shift appears to be second-order in ϵ. In addition, the frequency shift is always downward. We can explain both these effects through the mathematical framework we developed earlier.

Our system contains no perturbation to the sound speed, but now the Doppler term of equation (38) must be included when evaluating equation (30):

$$\oint k_z dz = \oint \left[\frac{(\omega_0 + \delta\omega - \mathbf{k}\cdot\mathbf{v})^2 - \omega_c^2}{c_0^2} - k_x^2 \right]^{1/2} dz = \pi, \tag{49}$$

where we have explicitly kept the line integral from equation (27). Performing the same expansion as done in §4.1 while treating $\mathbf{k}\cdot\mathbf{v}$ as a small parameter, we arrive at

$$\frac{\delta\omega}{\omega_0} = \left[\oint \frac{\mathbf{k}\cdot\mathbf{v}}{k_{z,0} c_0^2} dz \right] \left[\oint \frac{\omega_0}{c_0^2 k_{z,0}} dz \right]^{-1} \tag{50}$$

Again, we find that the frequency shift depends on the integral of the perturbation over the cavity. Since, as can be seen from Figure 3, the ray does not interact with all of the convective cell, we might expect the perturbation term not to average to zero. However, in this case the perturbation has an almost antisymmetric effect on rays propagating with and against the flow. To first order these shifts cancel, leaving $\delta\omega = 0$. However, we expect a non-zero second-order frequency shift, as can be shown by the following thought experiment. To first order, propagating with and against the velocity field produces equal and opposite Doppler shifts of the ray's frequency. But, the ray takes more time to traverse regions where the ray travels against the flow ($\mathbf{k}\cdot\mathbf{v} < 0$) than it does to cross regions where the ray and the flow are co-directional ($\mathbf{k}\cdot\mathbf{v} > 0$). The relative time difference is of order v/c and the value of the frequency shift is of order $-v/c$, leading to a net downward shift of order $-v^2/c^2$. This result is not restricted to the case considered here, but instead applies for any perturbation where the ray spends equal times, to first order, in

upshift and downshift regions. In particular, sound perturbations caused by the thermal structure of a convective call have this effect.

Instead of carrying out the expansion of equation (49) to second order in the small parameters, we can graphically demonstrate this result by varying the parameter ϕ of equation (48). By doing so, the resonant cavity will overlap different regions of the convective cell, leading to different frequency shifts. Near the top and bottom of each cell, the flow is predominantly horizontal. When the resonant cavity overlaps this region the horizontal component ($k_x v_x$) of equation (50) will produce the largest shift. Similarly, when the cavity overlaps regions of strong upflows and downflows, the vertical component ($k_z v_z$) will produce the strongest influence.

Figure 4 shows the relative frequency shift plotted versus the phase ϕ, for a $n = 1$, $\ell = 200$ mode with $z_c = 0.87$ and $\epsilon = 0.05$. The structure of the convective cells in equation (46) establishes that the plot is periodic outside the plotted range of $0 \leq \phi \leq \pi$. In this example, k_x is always larger than $|k_z|$ and so we expect the effects from the horizontal perturbation to be the strongest. The points $\phi = 0$ and $\phi = \pi$ correspond to configurations where the resonant cavity lies near the vertical intersection of two cells, and hence we would expect these points to show the largest perturbation, which is indeed the case. The minimum frequency shift is found, as expected, when $\phi = \pi/2$ since for this alignment of the cell and the resonant cavity the horizontal velocities sampled by the ray are smallest.

4.3. Convective Cell

While the cell studied in the preceding section was helpful in shaping our intuition, it was not particularly realistic. A more consistent model has sound speed and velocity perturbations in both the x and z directions. In this section we explore such a model and will show that the net frequency shift is still negative and second order in the strength of the perturbation.

Our reference state remains the adiabatically stratified, plane-parallel polytrope described above. We take our model for the convective state from Shirer (1987). It is a simple nonlinear model of steady Rayleigh-Bérnard convection derived from the Boussinesq equations in two dimensions. We work with the solution with the lowest mode numbers, two cells in the horizontal direction and one in the vertical.

After converting Shirer's parameterization to the notation of this paper, we are left with three free parameters: the depth of the convective cell z_T, the thermal diffusivity κ, and its product $\kappa\nu$ with the kinematic viscosity. Mindful of the constraint that the lengthscales of the fluid motions should be much larger than the lengthscales of the oscillation, we work with the largest possible convection cell, one the approximate depth of the solar convection zone, $z_T = 0.3 R_\odot$.

Estimates of κ and ν in the solar convection zone vary widely over a number of orders of magnitude. Our choice for these terms, however, does not have a physical motivation. Instead,

we choose these constants so that the size of the perturbations is kept small. A justification for this assumption comes from the observation that the solar convection zone is nearly adiabatically stratified, hence we expect the convective motions to be perturbations on the mean sound speed structure.

With these choices, the sound speed becomes

$$c^2 = \frac{gz}{\mu} + \alpha \cos\left(\frac{2\pi x}{L}\right) \sin\left[\pi\left(1 - \frac{z}{z_T}\right)\right] - \beta \sin\left[2\pi\left(1 - \frac{z}{z_T}\right)\right], \tag{51}$$

where $L = 2\pi R_\odot$ is the length of the cavity and α and β are functions of the product $\kappa\nu$. The velocity perturbations are given by

$$v_x = \gamma \sin\left(\frac{2\pi x}{L}\right) \cos\left[\pi\left(1 - \frac{z}{z_T}\right)\right] \qquad \text{and} \qquad v_z = \delta \cos\left(\frac{2\pi x}{L}\right) \sin\left[\pi\left(1 - \frac{z}{z_T}\right)\right], \tag{52}$$

where γ and δ are functions of κ and the product $\kappa\nu$. The nonlinear nature of the convection arises from the final term in equation (51) which is independent of x. For a linear cell, the perturbation would oscillate in x.

Specifically,

$$\alpha = \frac{gz_T}{\mu} \frac{\sqrt{8}}{\pi\,\mathrm{Ra}} \frac{a^2+1}{a} \left[\mathrm{Ra} - \mathrm{Ra}_c\right]^{\frac{1}{2}} \tag{53}$$

where

$$a = \frac{2z_T}{L} = \frac{0.3}{\pi}, \qquad \mathrm{Ra} = \frac{gz_T^3}{\kappa\nu\pi^4}, \qquad \text{and} \qquad \mathrm{Ra}_c = \frac{(a^2+1)^3}{a^2} \tag{54}$$

are the aspect ratio of the convective domain, the Rayleigh number, and the critical Rayleigh number for the onset of convection, respectively. The parameter β is defined by,

$$\beta = \frac{gz_T}{\mu} \frac{1}{\pi\,\mathrm{Ra}} \left[\mathrm{Ra} - \mathrm{Ra}_c\right] \tag{55}$$

We also have

$$\gamma = \frac{\pi\sqrt{8}}{z_T(a^2+1)} \kappa \left[\mathrm{Ra} - \mathrm{Ra}_c\right]^{\frac{1}{2}} \tag{56}$$

and

$$\delta = \frac{\pi\sqrt{8}a}{z_T(a^2+1)} \kappa \left[\mathrm{Ra} - \mathrm{Ra}_c\right]^{\frac{1}{2}} \tag{57}$$

From the expressions in equations (53)–(57) we can see that a critical parameter governing the sizes of the perturbation is

$$(\mathrm{Ra} - \mathrm{Ra}_c) = \left[\frac{gz_t^3}{\pi^4} \frac{1}{\kappa\nu} - \frac{(a^2+1)^3}{a^2}\right]. \tag{58}$$

In order to keep the perturbations small, we must choose the free parameters – κ and ν – such that this expression is small, but non-zero. For instance, choosing $\kappa\nu = 2.27$ and $\kappa = 0.1$ gives

$\mathrm{Ra} - \mathrm{Ra}_c = 9.5 \times 10^{-2}$, $\alpha = 0.50$, $\beta = 5.1 \times 10^{-3}$, $\gamma = 0.013$ and $\delta = 1.2 \times 10^{-3}$. Since we are exploring the parameter regime near the boundary of convective instability, small changes in the parameters can have large effects on the size of the perturbations.

Figure 5 shows the streamlines for the velocity profile given by equation (52) as well as the isotherms for the temperature perturbation given by the last two terms of equation (51). The standard picture of rising warmer fluid and sinking cooler fluid is seen to hold. As in Figure 3 the streamlines and isotherms close at depth and are linearly spaced.

This convective cell can be thought of as a combination of the perturbations considered in the two previous subsections. Comparison of the velocity perturbations of equations (52) and (47) show they are quite similar. We expect the perturbations arising from the velocity profile to be second-order by the argument advanced earlier. The sound speed perturbation of equation (51) is an interesting combination of a strong perturbation which we expect to enter the frequency shift at second order (the second term) due to its periodic horizontal structure and a small perturbation which will enter at first order (the third term). Our results show that it is difficult to separate the effects of these terms, at least in the parameter regime we are considering. The different runs are documented in Table 3 and show that the frequencies are downshifted and generally are of second order in the perturbation strength.

More interesting than the frequency shifts is the fate of the raypaths under the influence of this perturbation. As the most realistic model of convection under consideration, we expect that these raypaths will most closely approximate raypaths in the solar convection zone. Recall from Figure 1 that the raypaths and caustics for integrable systems are quite regular. We expect from the KAM theorem that for small perturbations the eigenrays will remain on invariant tori, implying that both the caustics and the raypaths will remain similar to, although possibly deformed from, the integrable shape. In addition, as the strength of the perturbation increases we expect the tori will eventually break down and the ray will begin to explore the entire coordinate space.

Figure 6 shows that both of these expectations are borne out. We have plotted sample raypaths for two different strengths of the convective perturbation. These raypaths were computed by running the raypath integration routine after adiabatic switching had completed, hence the frequency is constant in each panel. As in Figure 1, the horizontal structure of the ray has been altered for legibility. The top panel shows the raypaths for a weak perturbation and confirms our prediction that the ray will be confined to an invariant torus. The bottom panel shows the result from a stronger perturbation, the path of a ray which not confined to an invariant torus. If this integration was continued indefinitely, the ray would eventually diffuse onto a near-vertical trajectory and plunge out of the bottom of the displayed propagation region.

5. Discussion and Future Work

We have demonstrated how to compute frequency shifts arising from general perturbations with no special symmetries. From our investigations, we can draw some general conclusions concerning the effects of convection on p-mode eigenfrequencies. To first order, the relative frequency shift is roughly proportional to the integral of the perturbation over the resonant cavity of the eigenmode. For cases such as the sound speed perturbation considered in §4.1 where the perturbation is always either positive or negative, the shift is linear in the perturbation strength while the direction of the shift depends on its sign.

Of more physical interest is the case where the perturbation is not monotonic, but periodic. Here, we have shown through physical and mathematical arguments as well as numerical methods that the effect of the perturbation vanishes to first order. However, a second-order perturbation does exist which has a pleasing interpretation of being due to the extra time spent in regions of counter-propagating material. It is intriguing to note that, as discussed in Gough *et al.* (1996), the structure of present solar models near the top of the convection zone yields p-mode eigenfrequencies which are larger than those observed by helioseismology. This results of this paper show shifts in the proper direction; but, we have not yet shown that the second-order effect we discuss above is large enough to account for these differences.

In addition, we have demonstrated that even mild perturbations can significantly change the structure of an eigenmode's resonant cavity despite producing only small frequency shifts. As the perturbation strength increases, the ray eventually begins to move chaotically and is no longer confined in any obvious region. It is an open question whether this effect will persist when we investigate more realistic convective models. If it does, results from time-distance helioseismology imply that the ray parameterization does work in the Sun suggesting, perhaps, that consideration of average and not individual raypaths would be useful.

We have shown that adiabatic switching is a viable method of implementing the EBK quantization conditions for nonintegrable systems and finding the eigenfrequencies of simple convective envelopes in the WKB limit. For integrable systems where the eigenfrequencies can be directly computed from EBK quantization, adiabatic switching agrees quite well. Furthermore, adiabatic switching can find eigenfrequencies of non-integrable systems which are impractical to obtain through direct EBK quantization.

Adiabatic switching is an attractive method for finding eigenfrequencies, but care must be taken to apply it to problems for which it is valid. In the Sun, the true excited objects are global modes which are not necessarily well approximated by one-dimensional objects such as rays. Mathematically, one may approximate a ray whose dynamics are governed by equations (19) by superposing eigenmodes to form a wavepacket. But, Bogdan (1997) has shown that, due to the finite number of excited p modes, the smallest wavepacket which can be constructed by a coherent superposition in the Sun is ≈ 30 Mm. This dimension, characteristic of supergranules, suggests a lower size limit on the structures which can be explored using adiabatic switching. Smaller

structures are incompletely sampled by the wavepacket, suggesting that their effects are not fully realized. The smallest convective structures cannot be treated at all by WKB theory and their effects may well be modeled by turbulent pressure (Goldreich & Murray 1994, Gruzinov 1998).

Provided that they are of large enough scale, convective motions of almost arbitrary complexity can be investigated with adiabatic switching. A number of intriguing problems remain in this area including the exploration of other analytic models of convective structures such as upwellings and thermal plumes. We are not limited to analytic models, however. Numerical models of convection such as recent spherical shell simulations (Glatzmaier & Toomre 1995, Elliot *et al.* 1999) and convection in layers (Brummell *et al.* 1998) can also be studied with adiabatic switching.

Along with exploring convective structures, we can also investigate modifications to the dispersion relation of equation (38). A fairly simple conceptual, although perhaps computationally expensive, extension to this work would be to incorporate the third dimension into the plane-parallel geometry. The number of degrees of freedom would increase by one, however the reference system would remain integrable since another constant of the motion, k_y, would also be added. Perturbations analogous to the Doppler term of equation (38) can also be included. Both rotation and magnetic fields can be expressed as additional terms in the dispersion relation (Gough 1993).

Power spectra of the solar oscillations show that p modes possess an intrinsic line profile, the source and shape of which is not well understood. Previous works (Kumar *et al.* 1994, Roxburgh & Vorontsov 1995, Rast & Bogdan 1998) have treated the effects of intrinsic damping, noise, and source structure. Intriguingly, eigenfrequency linewidths are also generated by some of the effects we have explored in this paper. We ignored the inherent time-dependence of solar convection in this work; recall, however, that the frequency is a constant of the motion only for time-independent systems. Indeed, only by introducing $\lambda(t)$ into equation (35) could adiabatic switching work. In addition, the Sun is almost certainly not an integrable system, leading us to expect that a ray will diffuse in phase space as it propagates. Since the frequency is not a constant of the motion, its frequency can gradually change. We saw this effect in our work with non-integrable systems, but averaged results from several initial conditions to obtain a final result. Perhaps a closer exploration of the raw results will allow us insight into the nature of p-mode linewidths.

Finally, as a byproduct of using adiabatic switching, we generate multiple raypaths together with travel times for a given envelope. This library of paths could prove useful in investigations of time-distance helioseismology.

This work was supported by NASA GSRP 153-0972, NSF Grant AST-95-21779, the NASA Space Physics Theory Program, and the SOHO/MDI Investigation. We would also like to thank M. DeRosa, J. Weiss, R. Skodje, J. Meiss, and D. Haber for helpful discussions.

Table 1. Eigenfrequencies for the vertical sound speed perturbation of §4.1

n[a]	l[b]	ϵ[c]	κ[c]	$[\delta\omega/\omega]_{AS}$[d]	$[\delta\omega/\omega]_{EBK}$[e]
1[f]	200			3.5760	3.5760
2	200			4.2470	4.2470
1	400			5.0573	5.0573
1	200	0.01	0.10	8.5×10^{-4}	8.5×10^{-4}
2	200	0.01	0.05	5.9×10^{-4}	5.8×10^{-4}
1	400	0.01	0.05	2.0×10^{-4}	1.9×10^{-4}
1	200	0.01	0.05	4.1×10^{-4}	4.2×10^{-4}
1	200	0.02	0.05	8.4×10^{-4}	8.5×10^{-4}
1	200	0.04	0.05	1.7×10^{-3}	1.7×10^{-3}
1	200	0.08	0.05	3.4×10^{-3}	3.4×10^{-3}
1	200	0.16	0.05	6.8×10^{-3}	6.8×10^{-3}

[a]Vertical mode number from equation (31)

[b]Horizontal mode number from equation (33)

[c]Perturbation parameters from equation (40)

[d]Relative frequency shifts from adiabatic switching

[e]Relative frequency shifts from EBK quantization

[f]The first three rows give unperturbed frequencies for comparison purposes

Table 2. Eigenfrequencies for the velocity perturbation of §4.2

n[a]	l[b]	$\epsilon/R_\odot$[c]	ϕ[d]	$[\delta\omega/\omega]_{AS}$[e]
1	200	0.01	0.00	-9.6×10^{-5}
1	200	0.02	0.00	-3.8×10^{-4}
1	200	0.04	0.00	-1.4×10^{-3}
1	200	0.08	0.00	-5.5×10^{-3}
1	200	0.05	0.00	-2.1×10^{-3}
1	200	0.05	0.39	-2.0×10^{-3}
1	200	0.05	0.79	-1.6×10^{-3}
1	200	0.05	1.18	-1.3×10^{-3}
1	200	0.05	1.57	-1.2×10^{-3}
1	200	0.05	2.09	-1.4×10^{-3}
1	200	0.05	2.36	-1.6×10^{-3}
1	200	0.05	2.62	-1.8×10^{-3}
1	200	0.05	3.14	-2.1×10^{-3}

[a]Vertical mode number from equation (31)

[b]Horizontal mode number from equation (33)

[c]Perturbation parameter from equation (47)

[d]Perturbation parameter from equation (48)

[e]Relative frequency shifts from adiabatic switching

Table 3. Eigenfrequencies for the convective cell of §4.3

n[a]	l[b]	κ[c]	ν[d]	$[\delta\omega/\omega]_{AS}$[e]
1	200	0.1	22.7	-8.6×10^{-4}
1	200	0.05	45.4	-7.5×10^{-4}
1	200	0.01	227	-7.2×10^{-4}
1	200	0.1	22.6	-4.8×10^{-3}
1	200	0.05	45.2	-4.2×10^{-3}
1	200	0.01	226	-4.0×10^{-3}

[a]Vertical mode number from equation (31)

[b]Horizontal mode number from equation (33)

[c]Thermal diffusivity – see equations (53 - 57)

[d]Kinematic viscosity – see equations (53 - 57)

[e]Relative frequency shifts from adiabatic switching

REFERENCES

Arnol'd, V. I. 1978, Mathematical Methods of Classical Mechanics, Springer: New York

Bogdan, T. J. 1997, ApJ, 477, 475

Brillouin, L. 1926, J. Phys. Radium, 7, 353

Brown, T. M. 1984, Science, 226, 687

Brummell, N. H., Hurlburt, N. E., & Toomre, J. 1998, ApJ, 493, 955

Christensen-Dalsgaard, J., 1980, MNRAS, 190, 765

Cowling, T. G., 1941, MNRAS, 101, 367

Duvall, T. L. Jr., Jefferies, S. M., Harvey, J. W., & Pomerantz, M. A. 1993, Nature, 362, 430

Ehrenfest, P., 1917, Phil. Mag. 33, 500

Einstein, A. 1917, Verhandl. Deut. Physik. Ges.

Elliot, J. R., Miesch, M. S., Toomre, J., & Glatzmaier G. A. 1998, Structure and Dynamics of the Interior of the Sun and Sun-Like Stars, ed. by S. G. Korzennik and A. Wilson, ESA Publications Division: Noordwijk, in press

Glatzmaier, G. A., Toomre, J. 1995, Astron. Soc. Pac. Conf. Ser., 76, 200

Goldreich, P. & Murray, N. 1994, ApJ, 424, 480

Goldstein, H. 1965, Classical Mechanics, Addison-Wesley: Reading

Gough, D. O. 1993, Astrophysical Fluid Dynamics, ed. by J.-P. Zahn & J. Zinn-Justin, North-Holland: New York, 399

Gough, D. O., Kosovichev, A. G., Toomre, J., Anderson, E., Antia, H. M., Basu, S., Chaboyer, B., Chitre, S. M., Christensen-Dalsgaard, J., Dziembowski, W. A., Eff-Darwich, A., Elliott, J. R., Giles, P. M., Goode, P. R., Guzik, J. A., Harvey, J. W., Hill, F., Leibacher, J. W., Monteiro, M. J. P. F. G., Richard, O., Sekii, T., Shibahashi, H., Takata, M., Thompson, M. J., Vauclair, S., & Vorontsov, S.V. 1996, Science, 272, 1296

Gough, D. O., & Toomre, J. 1991, ARA&A, 29, 627

Gruzinov, A. V. 1998, ApJ, 498, 458

Hénon, M., & Heiles, C. 1964, AJ, 69, 73.

Johnson, B. R. 1985, J. Chem. Phys., 83, 1204

Keller, J. B. 1958, Ann. Phys., 4, 180

Keller, J. B., & Rubinow, S. I. 1960, Ann. Phys., 9, 24

Kumar, P., Goldreich, P., and Kerswell, R. 1994, ApJ, 427, 483

Landau, L. D., & Lifshitz, E. M. 1959, Fluid Mechanics, Pergamon: London, 256

Lavely, E. M., & Ritzwoller, M. H. 1993, ApJ, 403, 810

Lichtenberg, A. J., & Lieberman, M. A. 1983, Regular and Stochastic Motion, Springer-Verlag: New York

Noid, D. W., & Marcus, R. A. 1975, J. Chem. Phys., 62, 2119

Patterson, C. W. 1985, J. Chem. Phys., 83, 4618

Rast, M. P. & Bogdan, T. J. 1998, ApJ, 496, 527

Roxburgh, I. W. & Vorontsov, S. V. 1995, MNRAS, 272, 850

Shampine, L. F., & Gordon, M. K. 1975, Computer Solution of Ordinary Differential Equations, W. H. Freeman: San Francisco

Shirer, H. N. 1987, Nonlinear Hydrodynamic Modeling: A Mathematical Introduction, ed. by Shirer, H. N., Springer-Verlag: New York, 22

Shirts, R. B., Smiths, S. B., & Patterson, C. W., J. Chem. Phys., 86, 4452

Skodje, R. T., & Cary, J. R. 1988, Comput. Phys. Rep., 8, 221

Tabor, M. 1989, Chaos and Integrability in Nonlinear Dynamics: An Introduction, John Wiley & Sons: New York

Fig. 1.— Sample raypath in an adiabatically stratified, plane-parallel, horizontally-periodic envelope. The cavity has been horizontally compressed for clarity. Caustic surfaces at $z = 0.32$ and $z = 1.42$ are visible.

Fig. 2.— Relative perturbation to the sound speed described in equation (40). The dashed lines show the vertical extent of the ray's unperturbed cavity.

Fig. 3.— Streamlines for the velocity perturbation of §4.2 with $b = 3$. The streamlines connect at lower depth and the dashed lines show the resonant cavity of the intital ray.

Fig. 4.— Relative frequency shift versus the phase of the offset between the resonant cavity and the convective cell as defined in equation (48).

Fig. 5.— *Upper panel*: Streamlines for the convective perturbation described in §4.3. The streamlines connect at lower depths. The caustic surfaces of a sample raypath are shown as dashed lines. *Lower panel*: Temperature perturbation isotherms for the same convective structure.

Fig. 6.— *Upper panel*: Sample raypath for a weak convective perturbation ($\kappa = 0.01$, $\nu = 227$). As in Figure (1), the horizontal scale has been compressed for legibility. The deformed caustics are clearly visible. *Lower panel*: Raypath for a stronger perturbation ($\kappa = 0.1$, $\nu = 22.6$). The ray is no longer confined by caustics and will eventually explore all of coordinate space. Note the difference in vertical scales.

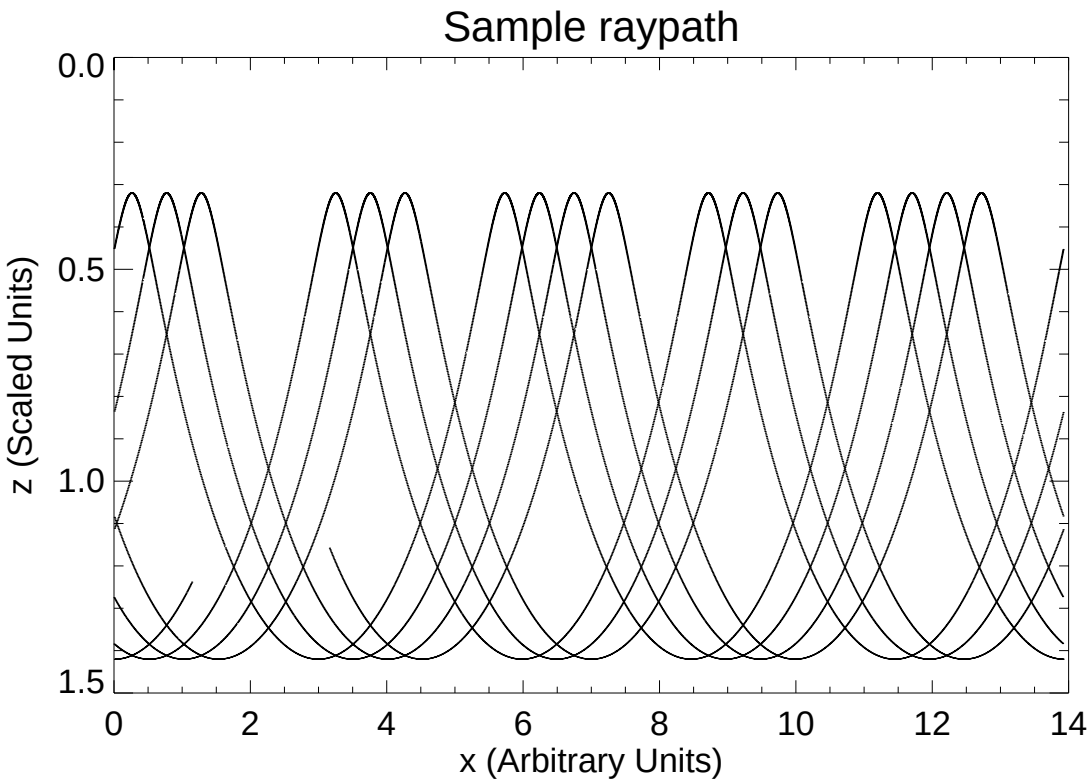
Sample raypath
z (Scaled Units)
0.0
0.5
1.0
1.5
0
2
4
6
8
10
12
14
x (Arbitrary Units)

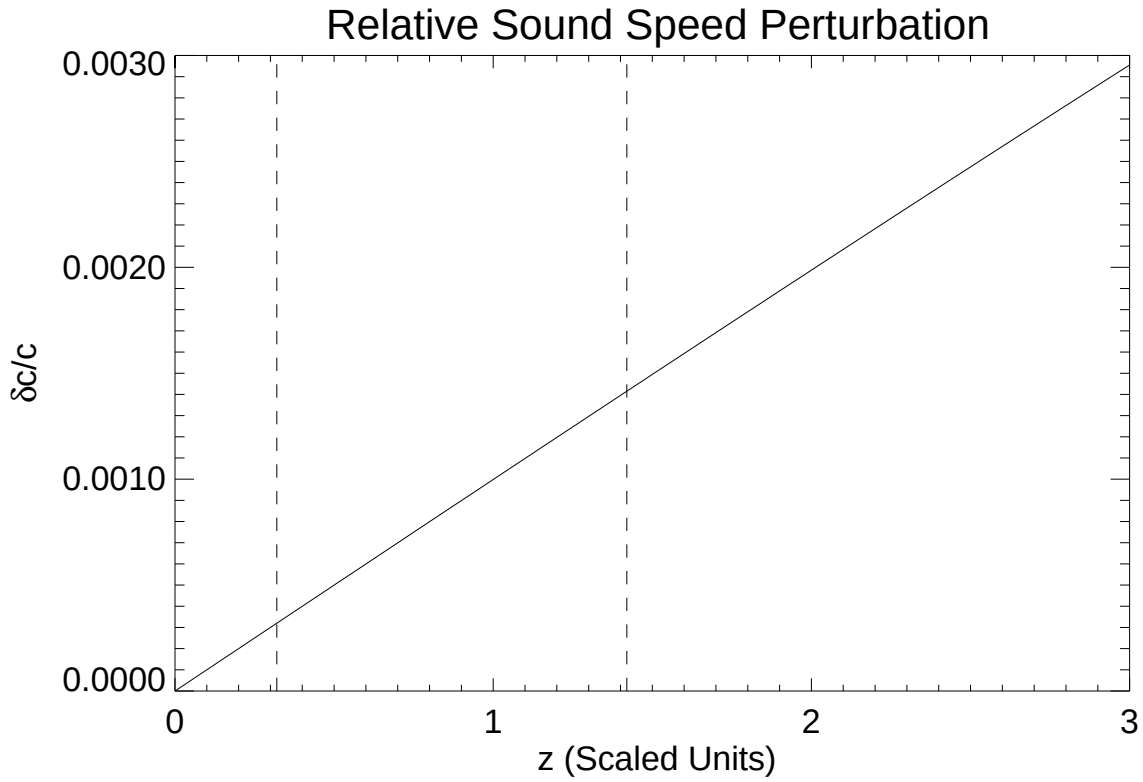
Relative Sound Speed Perturbation
0.0030
0.0020
0.0010
0.0000
δc/c
0
1
2
3
z (Scaled Units)

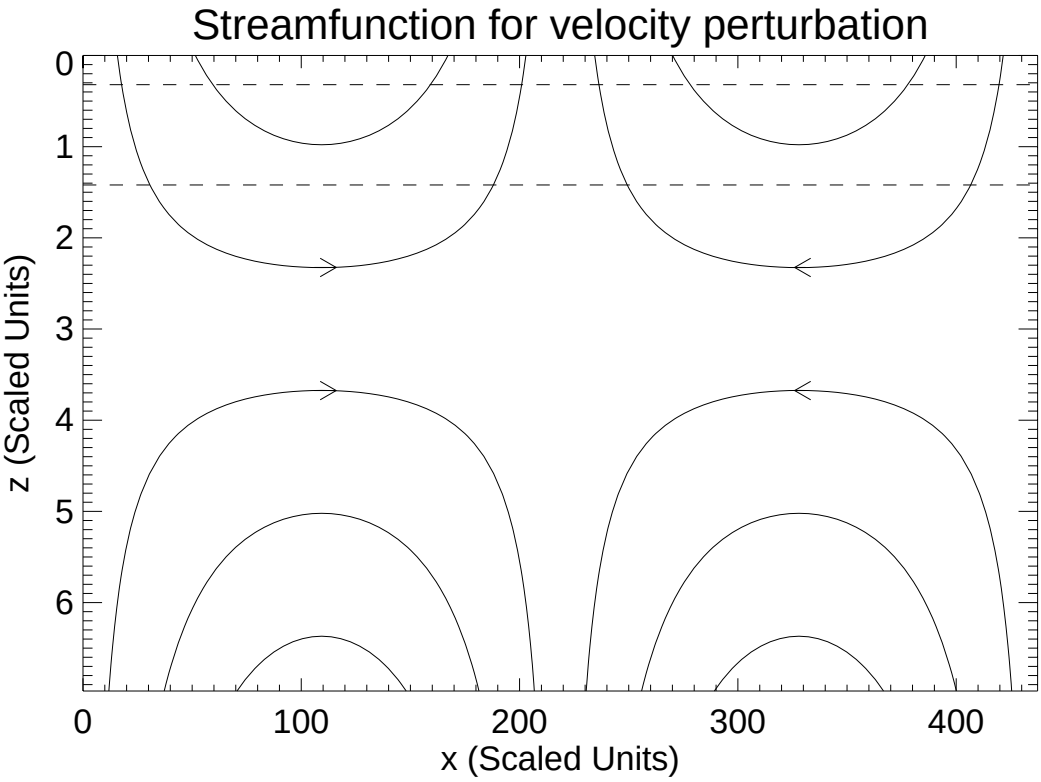
Streamfunction for velocity perturbation
z (Scaled Units)
0
1
2
3
4
5
6
0
100
200
300
400
x (Scaled Units)

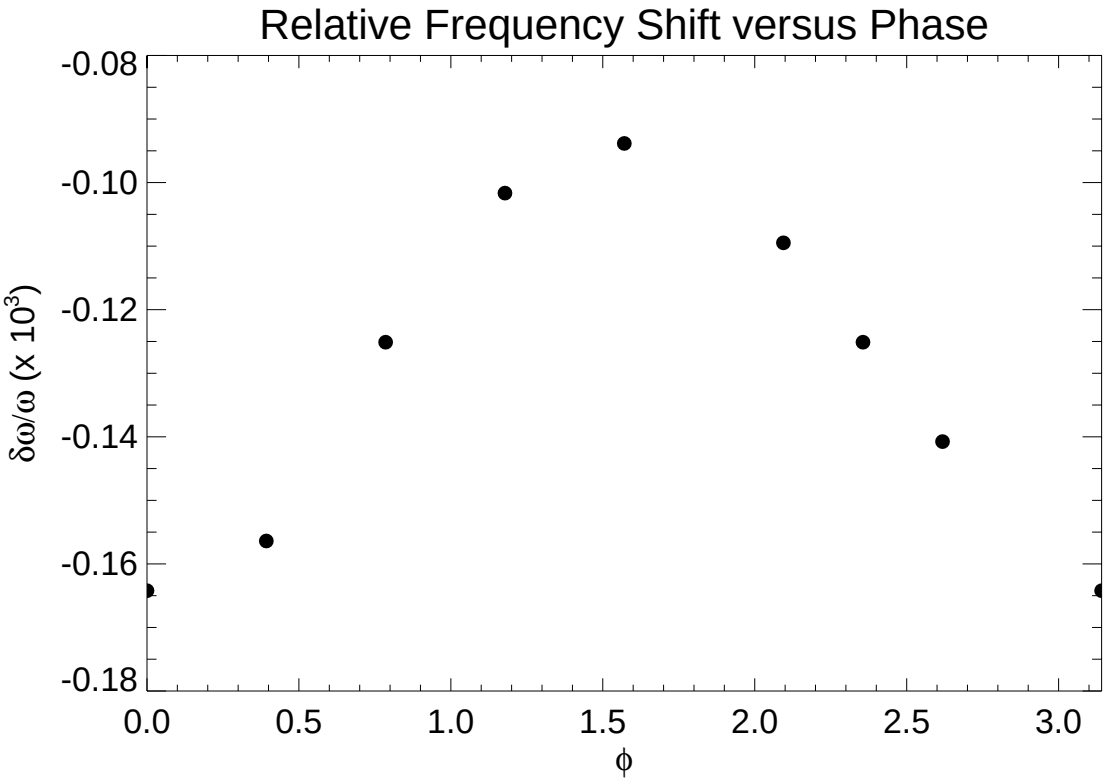
Relative Frequency Shift versus Phase
-0.08
-0.10
-0.12
-0.14
-0.16
-0.18
δω/ω (x 10^3)
0.0
0.5
1.0
1.5
2.0
2.5
3.0
ϕ

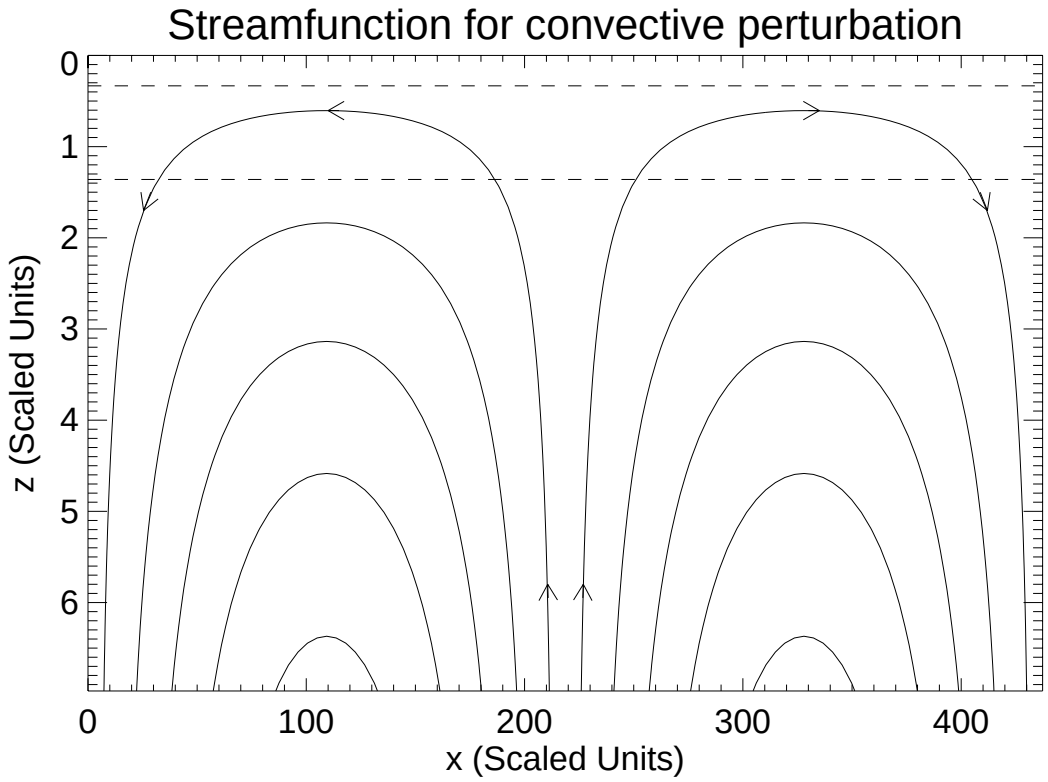
Streamfunction for convective perturbation
z (Scaled Units)
x (Scaled Units)
0
1
2
3
4
5
6
0
100
200
300
400

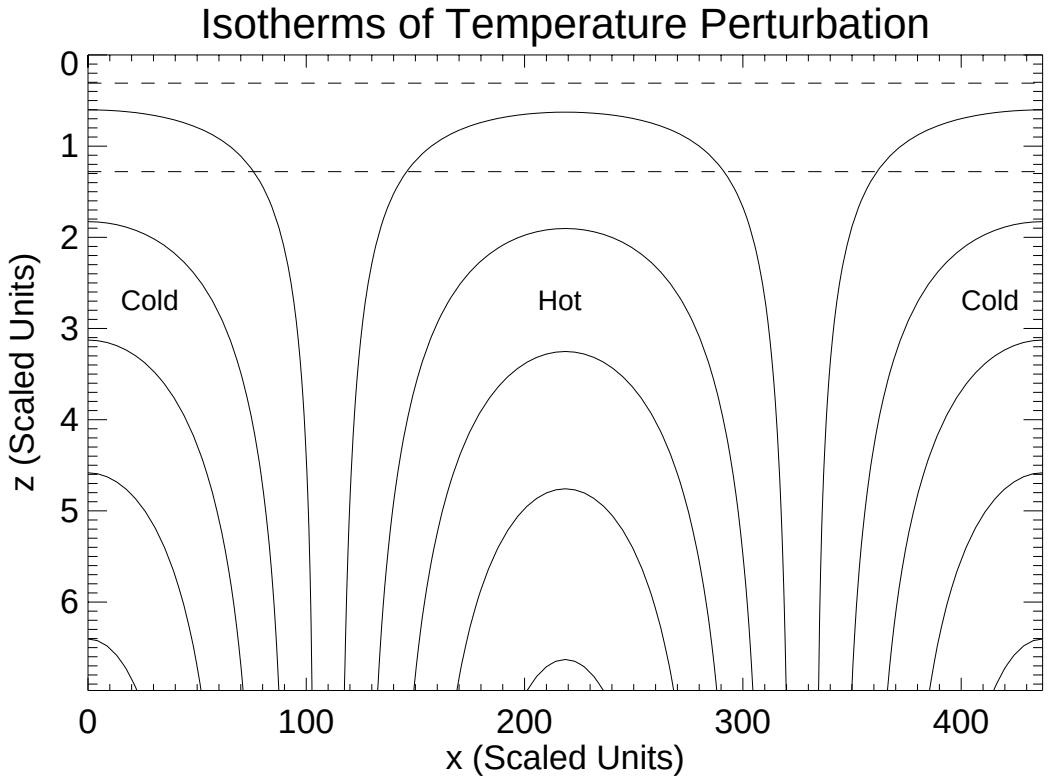
Isotherms of Temperature Perturbation
z (Scaled Units)
x (Scaled Units)
Cold
Hot
Cold
0
1
2
3
4
5
6
0
100
200
300
400

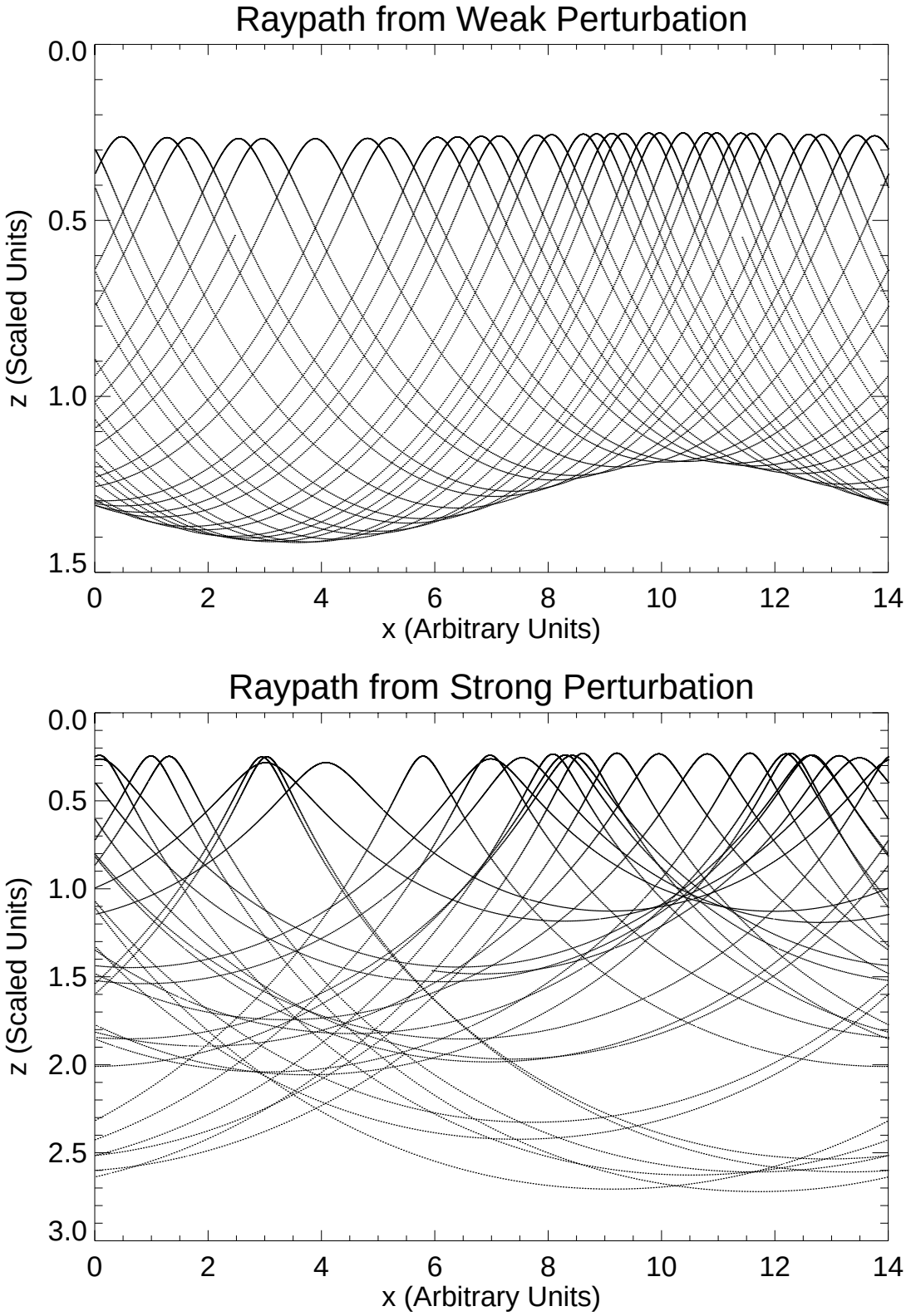
Raypath from Weak Perturbation
z (Scaled Units)
x (Arbitrary Units)
0.0
0.5
1.0
1.5
0
2
4
6
8
10
12
14
Raypath from Strong Perturbation
z (Scaled Units)
x (Arbitrary Units)
0.0
0.5
1.0
1.5
2.0
2.5
3.0
0
2
4
6
8
10
12
14